### Title

Soil properties and sediment accretion modulate methane fluxes from restored wetlands




### Journal

Global Change Biology, 24(9)

### ISSN

1354-1013



### Authors

Chamberlain, Samuel D
Anthony, Tyler L
Silver, Whendee L
et al.



### Publication Date

2018-09-01

### DOI

10.1111/gcb.14124

Peer reviewed

# Soil properties and sediment accretion modulate methane fluxes from restored wetlands

Samuel D. Chamberlain[1] | Tyler L. Anthony[1] | Whendee L. Silver[1] | Elke Eichelmann[1] | Kyle S. Hemes[1] | Patricia Y. Oikawa[2] | Cove Sturtevant[3] | Daphne J. Szutu[1] | Joseph G. Verfaillie[1] | Dennis D. Baldocchi[1]

[1] Department of Environmental Science, Policy, and Management, University of California, Berkeley, CA, USA [2] Department of Earth and Environmental Sciences, California State University, East Bay, Hayward, CA, USA [3] National Ecological Observatory Network, Battelle, Boulder, CO, USA

Correspondence Samuel D. Chamberlain, Department of Environmental Science, Policy, and Management, University of California, Berkeley, CA, USA.
Email: schamberlain@berkeley.edu

Abstract

Wetlands are the largest source of methane ($CH_4$) globally, yet our understanding of how process-level controls scale to ecosystem fluxes remains limited. It is particularly uncertain how variable soil properties influence ecosystem $CH_4$ emissions on annual time scales. We measured ecosystem carbon dioxide ($CO_2$) and $CH_4$ fluxes by eddy covariance from two wetlands recently restored on peat and alluvium soils within the Sacramento–San Joaquin Delta of California. Annual $CH_4$ fluxes from the alluvium wetland were significantly lower than the peat site for multiple years following restoration, but these differences were not explained by variation in dominant climate drivers or productivity across wetlands. Soil iron (Fe) concentrations were significantly higher in alluvium soils, and alluvium $CH_4$ fluxes were decoupled from plant processes compared with the peat site, as expected when Fe reduction inhibits $CH_4$ production in the rhizosphere. Soil carbon content and $CO_2$ uptake rates did not vary across wetlands and, thus, could also be ruled out as drivers of initial $CH_4$ flux differences. Differences in wetland $CH_4$ fluxes across soil types were transient; alluvium wetland fluxes were similar to peat wetland fluxes 3 years after restoration. Changing alluvium $CH_4$ emissions with time could not be explained by an empirical model based on dominant $CH_4$ flux biophysical drivers, suggesting that other factors, not measured by our eddy covariance towers, were responsible for these changes. Recently accreted alluvium soils were less acidic and contained more reduced Fe compared with the pre-restoration parent soils, suggesting that $CH_4$ emissions increased as conditions became more favorable to methanogenesis within wetland sediments. This study suggests that alluvium soil properties, likely Fe content, are capable of inhibiting ecosystem-scale wetland $CH_4$ flux, but these effects appear to be transient without continued input of alluvium to wetland sediments.

KEYWORDS: alternative electron acceptor, carbon flux, eddy covariance, greenhouse gas balance, information theory, peatland, redox, Sacramento–San Joaquin Delta

## 1 INTRODUCTION

Wetlands play a fundamental role in regulating global climate and are important biogeochemical hotspots, as they store ~18% of Earth's soil carbon (C; Lal, 2008), emit ~30% of global methane ($CH_4$) emissions (Kirschke et al., 2013; Saunois et al., 2016), while only occupying 5%–8% of the terrestrial land surface (Mitsch et al., 2013). Most wetlands are greenhouse gas (GHG) sinks over multicentury time scales due to carbon dioxide ($CO_2$) sequestration within anoxic soils, though they are commonly GHG sources over shorter time scales due to the high global warming potential of $CH_4$ they emit (Mitsch et al., 2013; Neubauer & Megonigal, 2015; Petrescu et al., 2015; Whiting & Chanton, 2001). Wetland C sequestration and $CH_4$ emissions are inextricably linked, as anoxic soil conditions inhibiting ecosystem respiration (ER) also activate archaeal $CH_4$ production (Conrad, 2009; Whalen, 2005), although recent studies suggest that significant $CH_4$ production also occurs in the oxic zone (Angle et al., 2017). The balance between these opposing fluxes primarily determines wetland GHG balances (Bubier & Moore, 1994; Hendriks, van Huissteden, Dolman, & van der Molen, 2007; Petrescu et al., 2015), and small differences in sustained ecosystem $CH_4$ emissions can induce large changes in wetland GHG exchange due to the >45-fold radiative forcing of $CH_4$ compared with $CO_2$ over decadal to centennial time horizons (Neubauer & Megonigal, 2015). Recent rises in atmospheric $CH_4$ have been attributed to a global increase in wetland $CH_4$ fluxes (Nisbet et al., 2016), and wetlands are currently the most uncertain component of the global $CH_4$ budget (Kirschke et al., 2013). A key driver of this uncertainty is a lack of ecosystem-scale flux measurements to better constrain models and improve our understanding of how process-level controls scale to whole ecosystem $CH_4$ emissions (Bridgham, Cadillo-Quiroz, Keller, & Zhuang, 2013; Saunois et al., 2016).

Methane fluxes from wetlands are governed by many interacting biophysical drivers, including temperature, C inputs, alternative electron acceptor pools, and water table depth (Bridgham et al., 2013). It is uncertain how these governing factors interact and scale to whole ecosystem fluxes due to sparse global coverage of ecosystem-scale eddy covariance flux sites (Petrescu et al., 2015), where current measurement campaigns may undersample relevant environmental gradients. Chamber flux syntheses have demonstrated that water table depth, temperature, vegetation, disturbance, and wetland type are important modulators of wetland $CH_4$ flux (Turetsky et al., 2014). A similar understanding of the controls on $CH_4$ fluxes is emerging from eddy covariance studies, where temperature (Chu et al., 2014; Hendriks, van Huissteden, & Dolman, 2010; Olson, Griffis, Noormets, Kolka, & Chen, 2013; Rinne et al., 2007; Wille, Kutzbach, Sachs, Wagner, & Pfeiffer, 2008), recent C inputs (Hatala, Detto, & Baldocchi, 2012; Morin et al., 2014),

wetland structure (Matthes, Sturtevant, Verfaillie, Knox, & Baldocchi, 2014; McNicol et al., 2017), vegetation cover (Morin et al., 2017; Rey-Sanchez, Morin, Stefanik, Wrighton, & Bohrer, 2017), and water table depth (Brown, Humphreys, Moore, Roulet, & Lafleur, 2014; Chamberlain, Boughton, & Sparks, 2015; Chamberlain et al., 2016; Chamberlain, Groffman, et al., 2017; Goodrich, Campbell, Roulet, Clearwater, & Schipper, 2015; Hendriks et al., 2007, 2010; Sturtevant et al., 2016) have been identified as dominant controls across many wetland ecosystems. Combined chamber and eddy covariance studies have further improved our understanding of how drivers of small-scale flux variation scale to ecosystem fluxes (Forbrich et al., 2011; Morin et al., 2017; Rey-Sanchez et al., 2017).

Small-scale field and laboratory studies have also demonstrated the influence of soil C content (Bridgham et al., 2013; Levy et al., 2012; Ye et al., 2016) and alternative electron acceptor pools, such as sulfate and ferric iron, on wetland $CH_4$ fluxes (Bridgham et al., 2013; Laanbroek, 2010; Miller, Lai, Friedman, Angenent, & Lipson, 2015; Poffenbarger, Needelman, & Megonigal, 2011). Recently, Holm et al. (2016) and Krauss et al. (2016) used eddy covariance to observe reductions in coastal wetland $CH_4$ fluxes with increasing salinity, speculatively due to sulfate redox inhibition of methanogenesis (Poffenbarger et al., 2011), demonstrating how redox conditions can modulate annual $CH_4$ emissions. Iron (Fe) minerals can also inhibit $CH_4$ production and emissions (Laanbroek, 2010), as observed in many laboratory and field studies (Ali, Lee, Lee, & Kim, 2009; Jäckel & Schnell, 2000; Neubauer, Givler, Valentine, & Megonigal, 2005; Teh, Dubinsky, Silver, & Carlson, 2008; Zhou, Xu, Yang, & Zhuang, 2014), although Fe inhibition to long-term ecosystem fluxes has not been documented by eddy covariance. Understanding the interactions between soil properties, such as Fe content, and $CH_4$ emissions may be particularly important to upscaling and modeling fluxes across complex, heterogeneous landscapes, such as river deltas or the tropics, the largest source of the global wetland $CH_4$ emissions (Kirschke et al., 2013), where high Fe concentrations influence rates of organic matter decomposition and $CH_4$ production (Dubinsky, Silver, & Firestone, 2010; Hall & Silver, 2013; Teh et al., 2008).

Wetland restoration and management programs have increasingly been proposed and implemented to mitigate climate change (Mitsch et al., 1998, 2013), and restoration strategies that minimize $CH_4$ emissions and maximize $CO_2$ uptake will provide the optimum climate benefit. These programs are particularly appealing in coastal ecosystems, where $CO_2$ sequestration rates are high and $CH_4$ flux rates are low (Conservation International, 2017; Poffenbarger et al., 2011), and in drained peatlands, where large $CO_2$ emissions from oxidizing peat can be reduced by re-flooding the landscape (Hatala, Detto, Sonnentag, et al., 2012; Knox et al., 2015; Wilson et al., 2016). A thorough understanding of $CH_4$ flux drivers is essential to these programs because the magnitude of $CH_4$ emissions may determine if

restored wetlands are a GHG source or sink (Knox et al., 2015). These emissions could affect funding of wetland restoration programs if financed through C markets alone (Oikawa, Jenerette, et al., 2017), though wetlands provide a number of relevant ecosystem services, such as nutrient retention, protection from storms and sea-level rise, and habitat preservation for wildlife (Hansson, Brönmark, Anders Nilsson, & Åbjörnsson, 2005; Swain, Boughton, Bohlen, & Lollis, 2013; Zedler & Kercher, 2005).

The Sacramento–San Joaquin Delta region of California (hereafter referred to as the Delta) is an area where financing of wetland restoration through California's Cap and Trade program is being considered. The Delta comprises a network of artificially drained islands reclaimed for agriculture, where the water table is maintained below sea level by active pumping and levees surrounding each island. Drainage began in the 1850s to facilitate agricultural development, and exposure of the highly organic soils has led to substantial land surface subsidence (Deverel & Leighton, 2010) and $CO_2$ emissions (Hatala, Detto, Sonnentag, et al., 2012; Knox et al., 2015), and wetland restoration efforts aim to accrete new sediments and reduce GHG emissions (Hatala, Detto, Sonnentag, et al., 2012; Miller, 2011; Miller, Fram, Fujii, & Wheeler, 2008). Prior to drainage, this region was a 2,990 $km^2$ tidal marsh where soils varied substantially across space due to fluvial deposition from major rivers that carried mineral alluvium from the Sierra Nevada mountain range to the Delta marshes (Atwater & Belknap, 1980; Atwater et al., 1979). These differences in predrainage wetland geomorphology give rise to a contemporary agricultural landscape where large changes in soil C and mineral content occur over small spatial scales (Soil Survey Staff, 2017), but how this edaphic variation influences current GHG fluxes from restored wetlands is unknown. Understanding the importance of these soil legacy effects is highly desirable, as it would allow for more informed wetland restoration strategies where sites could be chosen to minimize GHG emissions.

The objectives of this study were to (1) determine how soil properties and wetland GHG fluxes varied across wetlands restored on peat vs. alluvium soils, (2) identify how relationships between biophysical drivers and $CH_4$ fluxes varied across wetland types, and (3) determine the most likely drivers (climate vs. edaphic) of observed flux differences. To meet these objectives, we measured ecosystem-scale $CH_4$ and $CO_2$ fluxes by eddy covariance from two recently restored wetlands, where one wetland was restored on peat soils while the other was restored on alluvium soils, and measured multiple soil properties within the tower footprints to identify potential edaphic drivers of observed flux differences. Soil properties were measured across two horizons as a proxy for time, and this depth for time assumption is valid because vertical accretion of new sediments in Sacramento–San Joaquin Delta wetlands has been documented using both feldspar marker (Miller et al., 2008) and radiocarbon dating methods (Drexler, 2011; Drexler, de Fontaine, & Brown, 2009). We then used a combination of wavelet analysis

and information theory to identify time scale-emergent biophysical drivers of $CH_4$ fluxes and how they varied across the wetlands. Once differences were established, we used an empirical biophysical $CH_4$ flux model trained on an independent mature wetland to determine whether observed differences could be explained by common, nonedaphic biophysical drivers alone. These tower sites are ideal for identifying edaphic controls, as all wetlands sites have a similarly managed hydroperiod, are within 13 km of one another, experience the same climate, and have similar plant community compositions.

## 2 MATERIALS AND METHODS

### 2.1 Site description

We measured wetland ecosystem $CH_4$ and $CO_2$ fluxes using a network of eddy covariance towers in the Sacramento–San Joaquin Delta region of California, USA. The Delta is located within a Mediterranean climate that experiences hot, dry summers and cooler, rainy winters. The mean annual temperature is 15.1°C (1998–2015 average), and the region receives 326 mm of rainfall annually (Knox et al., 2016). All measurement sites were located on Sherman and Twitchell Islands in the northwest Delta. These islands are a mosaic of alluvium mollisols and highly organic peat histosols (Soil Survey Staff, 2017). Alluvium marsh mollisols frequently developed adjacent to peat histosols that were spatially segregated from the main river channels (Atwater & Belknap, 1980; Atwater et al., 1979). Alluvium soils formed via fluvial deposition from major rivers and are most common on islands adjacent to the Sacramento River compared with the central and eastern Delta region where fluvial deposition was less pronounced (Deverel & Leighton, 2010). These alluvium soils tend to be high in Fe content, as the Sacramento River drains the northern Sierra Nevada range where Fe concentrations are particularly high compared with the central or south Sierra Nevada (Graham & O'Geen, 2010). In contrast, peat histosols formed densely organic soils in areas less disturbed by fluvial input (Deverel & Leighton, 2010). The dominant mollisol series on these islands are Gazwell and Scribner (Figure 1), both of which are formed in mixed alluvium, belong to the soil class Cumulic Endoaquolls, and are only found on Delta islands within the Sacramento River drainage (Soil Survey Staff, 2017). Rindge is the major histosol series found on both islands (Figure 1) and is widely distributed across the Delta region. Rindge soils belong to the Typic Haplosaprists class and are characterized by deep, poorly drained marsh soils formed from decomposed plant organic matter (Soil Survey Staff, 2017).

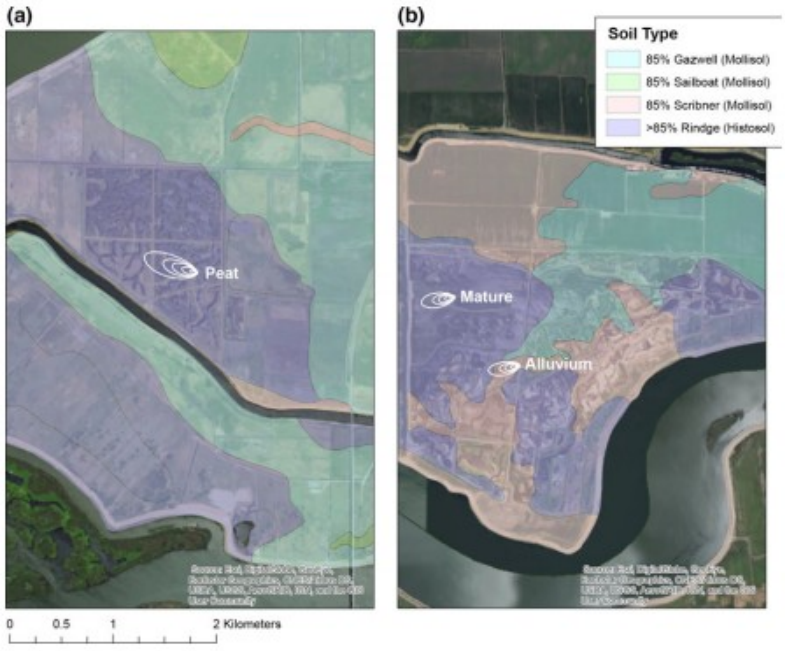


**FIGURE 1** Soil type and tower flux footprints for (a) Sherman and (b) Twitchell Islands in the Sacramento–San Joaquin Delta of California. Tower footprints include wetland area only, and footprint rings, from largest to smallest, correspond to the 90%, 85%, 80%, 70%, and 50% cumulative flux footprints at each site. Tower footprints were calculated using a two-dimensional analytical model described in Detto et al. (2006). Site names are given next to their respective footprint

Fluxes were measured from the time of initial restoration at two sites, where one wetland, hereafter referred to as the “peat” site (Ameriflux site Us-Myb; N38.0498, W121.7650), was restored in 2010 from a pasture on peat Rindge soils (Figure 1a). The other recently restored site, hereafter referred to as the “alluvium” site (Ameriflux site US-Tw4; N38.10275, W121.64125), was restored in 2014 from a corn field on alluvium Scribner soils (Figure 1b). We have also measured fluxes since 2013 from an older, mature wetland, hereafter referred to as the “mature” site (Ameriflux site Us-Tw1; N38.1074, W121.6469), that was restored in 1999 on peat Rindge soils (Figure 1b). A detailed description of tower instrumentation can be found in the Supporting Information and Eichelmann et al. (2018). All sites are vegetated predominantly by cattails (*Typha* spp.), with few tules (*Schoenoplectus acutus*), and are actively managed to remain inundated year-round. Peat and alluvium sites were constructed to have heterogeneous bathymetry, providing channels of open water and areas of closed vegetation. The mature site is entirely closed vegetation and the ground surface is saturated plant detritus, whereas the recently restored peat and alluvium sites have standing water under the plant canopy (Eichelmann et al. 2018). Given the large differences age and stand structure between the mature wetland and other sites, most comparisons made in this study are between the recently restored peat and alluvium sites that have similar bathymetry, stand structure, and measurement coverage across early successional periods. For a more detailed description of the wetland sites, see Miller (2011), Matthes et al. (2014), and Eichelmann et al. (2018).

Flux corrections and quality control were applied as described in detail in Knox et al. (2015) and Chamberlain, Verfaillie, Eichelmann, Hemes, and

Baldocchi (2017), and included high-frequency data despiking, 2-D coordinate rotations, density corrections, and site-specific friction velocity ($u^*$) filtering. At the mature site, we reject fluxes from wind directions 290°–240° because fluxes from these directions were from other wetland types; however, we did not apply wind direction filtering to the other sites where flux footprints were more homogeneous. Footprints at all sites were calculated using a two-dimensional analytical model (Detto, Montaldo, Albertson, Mancini, & Katul, 2006; Hsieh, Katul, & Chi, 2000).

We gap filled missing fluxes using artificial neural networks (ANNs), as described in detail in Knox et al. (2015). Briefly, we used single-layer, feed-forward ANNs with meteorological variables as inputs. Flux data without missing values were split into training, validation, and test sets (1/3 split), and we trained multiple ANN architectures with varying nodes per single hidden layer, keeping the simplest architecture where a more complex architecture led to a less than 5% reduction in root mean squared error (RMSE). This process (including resampling training, validation, and test data) was repeated 20 times, and the median of the 20 ANN predictions was used to fill missing fluxes and the variance was used to estimate gap filling uncertainty. Separate ANNs were trained for daytime and nighttime $CO_2$ fluxes, and the nighttime $CO_2$ flux ANN was used to model ER at all times. Gross ecosystem photosynthesis (GEP) was then estimated as the difference between the gap-filled $CO_2$ flux and modeled ER (Baldocchi & Sturtevant, 2015). Our partitioning method performs well against independent verification methods in agricultural systems (Oikawa, Sturtevant, et al., 2017).

## 2.2 Soil analyses

We measured soil C, N, and Fe content at the three wetland sites in the recently accreted wetland O horizon, hereafter referred to as the accreted horizon, and the underlying pre-restoration parent soils, hereafter referred to as the parent horizon. Fifteen samples of both accreted and parent horizon soils were collected at each site across three transects, with each sampling location at least 3 m apart. The transects were within each tower's flux footprint, all samples were collected from fully inundated locations, and the accreted sample was collected directly above the underlying parent soil sample. At the peat and alluvium sites (both <8 years old), the differentiation between these horizons was clear, as the recently accreted horizon was loose, mucky, and heavily comprised poorly decomposed plant matter, whereas the underlying parent horizon was compacted agricultural soil. At these sites, we collected the accreted horizon by hand (grab samples) and the top 15 cm of parent horizon using a sediment core. Our sampling strategy was different at the mature site because more than 0.5 m of O horizon had accumulated since initial restoration. Here, the accreted horizon reached the water surface, and we collected the top 2 cm of this horizon to represent the most recently accreted peat. We then bore holes through the 0.5–0.7 m saturated peat layer to collect the underlying parent soil horizon.

Differentiation between these layers was also clear, as the top 0.5–0.7 m comprised poorly decomposed plant matter and the underlying horizon was a silty clay loam. These observations are consistent with previously measured accretion rates and peat depths (Miller et al., 2008).

All soil samples were immediately bagged, and subsamples were extracted in the field with both 0.5 M HCl and 0.2 M sodium citrate/0.05 M sodium ascorbate solutions to measure HCl extractable Fe ($Fe^{2+}$ and $Fe^{3+}$) and poorly crystalline Fe oxide pools, respectively. The HCl extraction solubilizes reactive $Fe^{3+}$ minerals and absorbed/solid $Fe^{2+}$ and is used to quantify oxidized ($Fe^{3+}$) and reduced ($Fe^{2+}$) Fe pools. The low pH of HCl prevents any $Fe^{2+}$ oxidation after the samples are collected (Hall & Silver, 2015). Roughly 3 g of sample (dry mass equivalent) was immediately placed into preweighed bottles with the HCl solution, and once back in the lab, samples were reweighed, vortexed, shaken for 1 hr, and centrifuged for 10 min at 1,000 rcf. Concentrations of $Fe^{2+}$ and $Fe^{3+}$ were measured colorimetrically using the ferrozine assay (Viollier, Inglett, Hunter, Roychoudhury, & Van Cappellen, 2000). Citrate-ascorbate extractions were used to quantify poorly crystalline Fe oxides that are reducible by soil microbes (Hyacinthe, Bonneville, & Van Cappellen, 2006). Roughly 1.5 g of sample (dry mass equivalent) was immediately placed into preweighed bottles of the citrate-ascorbate solution, and in the lab, samples were reweighed, vortexed, shaken for 16 hr, and then centrifuged for 20 min at 1,000 rcf. Poorly crystalline Fe concentrations were quantified using an inductively coupled plasma optical emission spectrometer (ICP-OES; Perkin Elmer Optima 5300 DV, Waltham, MA, USA). We then air-dried soil samples at room temperature for analysis of C and N concentrations. Dried subsamples were sieved to 2 mm and all major visible roots were removed by hand. These samples were then ground to a fine powder and analyzed in duplicate for total C and N using an elemental analyzer (CE Elantech, Lakewood, NJ, USA).

### 2.3 Wavelet-information theory analysis

We used a combination of wavelet time series decomposition and information theory to (1) isolate major time scales of variation within the continuous $CH_4$ flux time series and (2) identify scale-emergent interactions between $CH_4$ fluxes and a number of biophysical drivers. This technique allowed us to isolate $CH_4$ flux controls operating at hourly, diel, and multiday timescales, and has been previously used to identify scale-emergent controls of $CH_4$ flux at the peat and mature wetlands (Sturtevant et al., 2016). Relative mutual information ($I^R$), an information theory metric, was used to identify relationships between variables. Mutual information is derived from Shannon entropy ($H$), a measure of uncertainty (Shannon & Weaver, 1998), and $I^R$ quantifies the amount of information shared between two variables. Mutual information and other information theory metrics, such as transfer entropy, are particularly useful for identifying relationships in complex systems because they do not assume linearity or other functional relationships and are capable of identifying asynchronous relationships

(Ruddell, Brunsell, & Stoy, 2013). All wavelet decomposition and entropy calculations were conducted using the ProcessNetwork Software (http://www.mathworks.com/matlabcentral/fileexchange/41515-processnetwork-processnetwork-software), and a more detailed description of the approach can be found in the Supporting Information and Sturtevant et al. (2016).

### 2.4 Statistical analyses and data processing

All additional data processing, statistical analysis, and visualization were conducted in R 3.4.1 (R Core Team, 2017) using the "tidyverse" (Wickham, 2017), "zoo" (Zeileis & Grothendieck, 2005), "gridExtra" (Auguie, 2016), "ggpubr" (Kassambara, 2017), "lubridate" (Grolemund & Wickham, 2011), and "scales" (Wickham, 2016) packages. We used parametric statistics, such as ANOVA, Welch's *t* tests, and Tukey's HSD, to assess differences in soil properties across/within sites because properties were normally distributed within soil horizons at each site. Annual GHG budgets were calculated using the 45× 100-year sustained-flux global warming potential for $CH_4$ presented in Neubauer and Megonigal (2015).

We also analyzed the residuals of a generalized linear model (GAM) fit to daily $CH_4$ fluxes at the mature wetland (2014–2017) using nine common biophysical drivers (described in Results) to assess whether changes in alluvium $CH_4$ fluxes with time could be explained by common, nonedaphic drivers of stable state wetland $CH_4$ flux. The GAM was fit using the "caret" (Kuhn, 2017) and "mgcv" (Wood, 2017) R packages, where smoothing parameters were chosen by generalized cross-validation and inclusion of feature selection was chosen by using the model formulation with the lowest RMSE following tenfold cross-validation. The trained GAM was then used to predict $CH_4$ fluxes at the peat and alluvium wetlands. Prior to model training and prediction, missing values in the biophysical driver data were imputed using k-nearest neighbors, where all values were centered and scaled. This manuscript is reproducible via R Markdown, and its code can be found at https://github.com/samdchamberlain/wetlandcomparison. The wavelet-information theory analysis was conducted using MATLAB and is not directly reproducible in R; however, MATLAB source code (https://github.com/samdchamberlain/ProcessNetwork_Software) is available online.

## 3 RESULTS

### 3.1 Soil properties

Extractable Fe concentrations were significantly higher in recently accreted and parent alluvium soil horizons compared with those at the peat wetland (Tukey's HSD, $p < .001$; Figure 2a). Extractable Fe concentrations trended lower in the accreted compared with parent horizon at both wetlands, but these differences were not significant (Figure 2a). Appreciable quantities of $Fe^{3+}$ were present in all site horizons, where 28.0% and 33.9% of extractable

Fe were in $Fe^{3+}$ form at the alluvium and peat sites, respectively. Most Fe was in the reduced $Fe^{2+}$ form across both sites, and statistical trends in $Fe^{2+}$ concentrations were similar to total extractable Fe (Figure 2b). While total extractable Fe concentrations did not vary between horizons at the alluvium site, $Fe^{2+}$ concentrations were significantly higher in the accreted horizon compared to its underlying parent soil (Welch's $t$, $p < .001$).

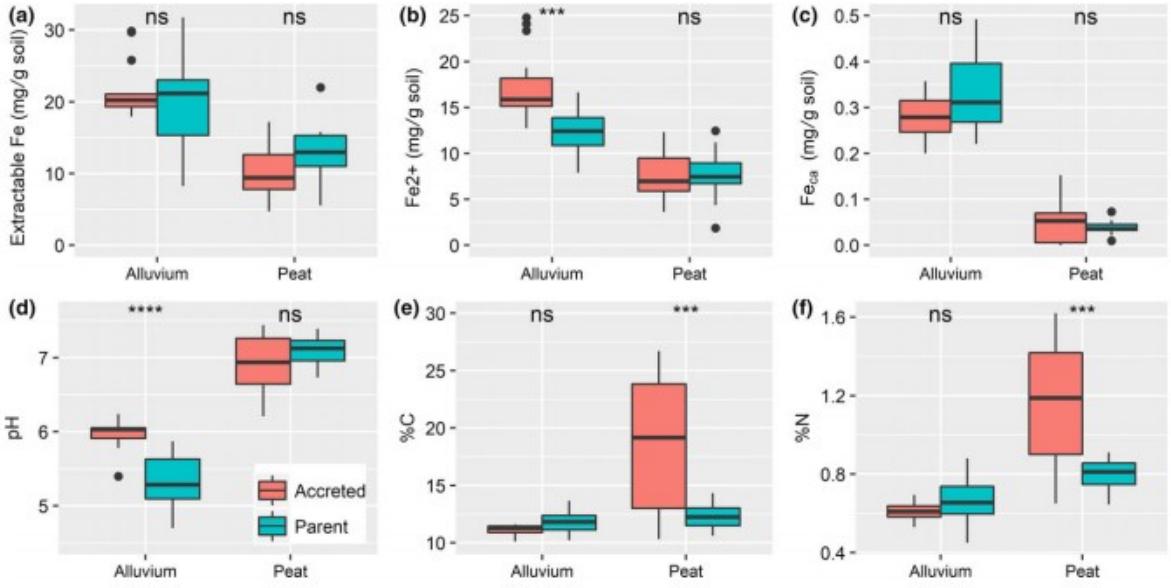


**FIGURE 2** Soil (a) HCl-extractable Fe, (b) ferrous iron ($Fe^{2+}$), (c) poorly crystalline Fe oxides ($Fe_{ca}$), (d) pH, (e) C concentration (%), and (f) N concentration (%) in accreted and parent horizons across the peat and alluvium wetlands ($n \geq 12$ per depth). Solid horizontal lines are medians, boxes are the interquartile range, whiskers are the 95% confidence interval, and points denote measured outliers. Significance levels are shown for pairwise comparisons between soil horizons at each site (Welch's $t$ test), where ns denotes no significant differences and increasing asterisks denotes significance levels from $p < .05$, .01, .001, to .0001

Poorly crystalline Fe oxide concentrations were roughly two orders of magnitude lower than HCl-extractable Fe concentrations across both sites (Figure 2c), and trends were similar to HCl-extractable Fe. Poorly crystalline Fe concentrations were significantly higher at the alluvium site in both soil horizons (Tukey's HSD, $p < .0001$) and did not vary between horizons at either wetland (Figure 2c). Mean poorly crystalline Fe concentrations were roughly an order of magnitude higher in alluvium soils (0.32 ± 0.09 mg Fe/g soil; $n = 30$) compared with peat soils (0.04 ± 0.04 mg Fe/g soil; $n = 30$).

Soil pH also varied across the wetlands (ANOVA, $p < .05$), where alluvium soils were acidic (5.62 ± 0.48; $n = 30$) and peat soils were near-neutral (6.99 ± 0.33; $n = 28$; Figure 2d). pH did not vary by depth at the peat wetland; however, the parent horizon was significantly more acidic at the alluvium wetland (Welch's $t$, $p < .0001$; Figure 2d).

Parent horizon C concentrations did not vary between the peat and alluvium wetlands (Tukey's HSD, $p = .50$; Figure 2e). Significant differences in C concentrations were observed in the accreted horizon (Tukey's HSD, $p < .0001$), where C concentrations were higher at the peat site (15.64 ± 5.23%; $n = 14$) than the alluvium site (10.18 ± 1.49%; $n = 15$). Soil C concentrations

were higher in the recently accreted horizon at the peat site (Welch's $t$, $p <$ .001), but no differences in C concentration were observed between horizons at the alluvium wetland (Figure 2e). Similar patterns were observed for soil N concentrations across sites; however, parent horizon N concentrations were significantly lower at the alluvium compared with peat site (Tukey's HSD, $p =$ .01; Figure 2f).

### 3.2 Postrestoration flux trajectories

Methane flux trajectories from the peat and alluvium wetlands were quite different following initial restoration, where flux magnitudes were considerably lower from the alluvium site for the first 3 years following restoration and later converged with the peat site (Figure 3a). Across both sites, in the first-year wetlands were open water and nonvegetated, leading to low $CH_4$ flux and *NEE* compared to following years (Figure 3), and by the second year both sites were fully vegetated. Alluvium wetland fluxes increased with each year, whereas $CH_4$ fluxes from the peat wetland peaked during the second year and decreased with subsequent years (Figure 3a). Differences in daily fluxes across wetlands were largest during the second year when alluvium wetland fluxes were increasing and peat wetland emissions were peaking (Figure 3a). Annual $CH_4$ budgets for the peat site were over two times larger than the alluvium site during the first and second years. First-year budgets were 16.4 ± 2.2 and 35.6 ± 4.2 g $CH_4$-C $m^{-2}$ $year^{-1}$ (mean ± 95% CI) for the alluvium and peat wetland, respectively, and second-year budgets were 27.8 ± 2.5 and 63.4 ± 3.6 g $CH_4$-C $m^{-2}$ $year^{-1}$ for the alluvium and peat wetland, respectively. This gap began to close during year 3, and fluxes were similar across sites by year 4 (Figure 3a), when annual fluxes were 49.2 ± 3.7 and 57.2 ± 3.5 g $CH_4$-C $m^{-2}$ $year^{-1}$ from the alluvium and peat wetland, respectively.

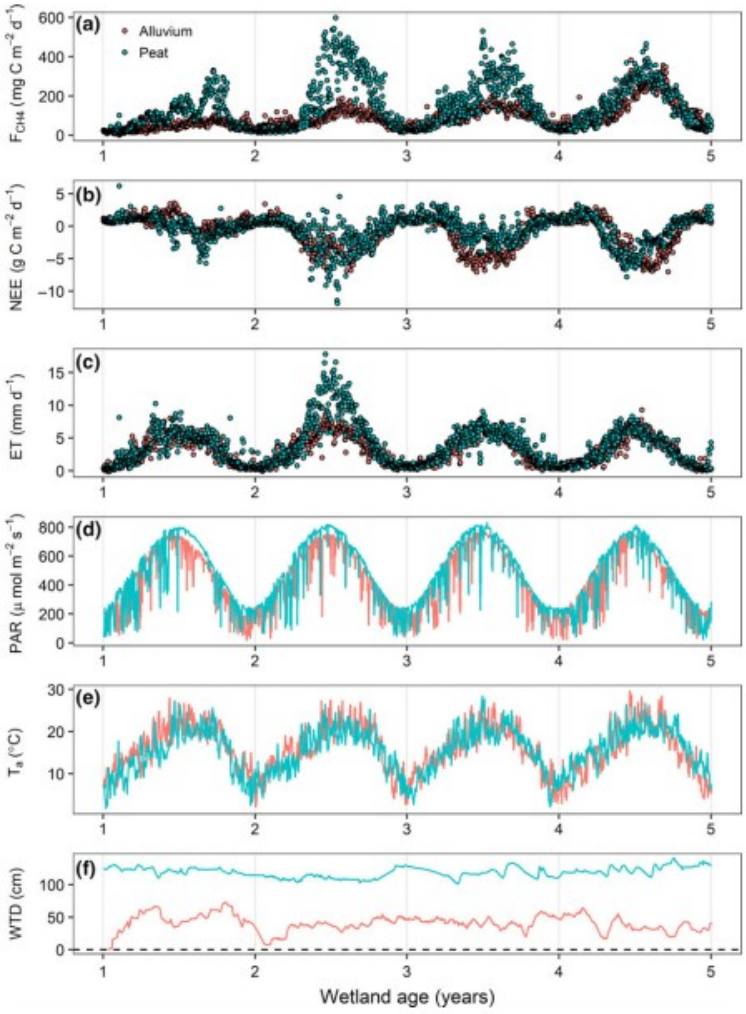


**FIGURE 3** Daily (a) methane flux ($F_{CH4}$), (b) net ecosystem exchange (NEE), (c) evapotranspiration (ET), as well as mean (d) photosynthetically active radiation (PAR), (e) air temperature ($T_a$), and (f) water table depth (WTD) at the peat and alluvium wetland from time since initial restoration. Day 1 is 2011-01-01 for the peat wetland and 2014-01-01 for the alluvium wetland

Differences in NEE were less notable across the two recently restored wetlands and did not follow similar trends to $CH_4$ flux. Daily NEE was similar across the two wetlands during the first and second years (Figure 3b), and annual budgets did not differ across the two sites during these years. First-year budgets were 262.3 ± 118.6 and −3.4 ± 180.1 g C m$^{-2}$ year$^{-1}$, and second-year budgets were −556.0 ± 112.8 and −449.0 ± 201.9 g $CO_2$-C m$^{-2}$ year$^{-1}$ for the alluvium and peat wetland, respectively. During year 3, the peat wetland sequestered less $CO_2$ despite emitting more $CH_4$ compared with the alluvium wetland (Figure 3b). Here, annual NEE was significantly less from the peat wetland (−37.5 ± 139.2 g $CO_2$-C m$^{-2}$ year$^{-1}$) compared with the alluvium wetland (−546.9 ± 105.0 g $CO_2$-C m$^{-2}$ year$^{-1}$). Similar to $CH_4$ fluxes during year 4, daily NEE was roughly equivalent between the two recently restored sites, though the onset of $CO_2$ uptake varied (Figure 3b).

Other dominant biophysical drivers of GHG fluxes, including evapotranspiration (ET), photosynthetically active radiation (PAR), air temperature ($T_a$), and water table depth (WTD), were similar across the wetlands, despite measurements occurring across different time periods

(2011–2014 for the peat site; 2014–2017 for the alluvium site). Daily ET exhibited a similar seasonality and magnitude across sites, with the exception of the second year at the peat wetland when particularly large ET rates were observed (Figure 3c). Daily mean PAR and $T_a$ were also similar across the wetlands during these time periods, and values generally overlapped in range (Figure 3d,e). In addition, the water table was always above surface at either wetland for the first 3 years following restoration and is, therefore, not responsible for reduced $CH_4$ fluxes at the alluvium wetland (Figure 3f).

### 3.3 Biophysical drivers of $CH_4$ flux

During the second-year postrestoration when differences in $CH_4$ flux magnitudes between the peat and alluvium wetland were largest (Figure 3a) and both wetlands were fully vegetated, $CH_4$ flux patterns and their relations to biophysical drivers were notably different across sites (Figure 4). Methane fluxes from the peat wetland during year 2 (2012) were strongly coupled to plant processes across multiple time scales (Figure 4a,c,e). At the hourly time scale, $CH_4$ flux shared most information with ET (Figure 4a), and at the diel scale, dominant interactions were synchronous and related to plant processes, such as ET, NEE, and gross ecosystem photosynthesis (GEP) as well as wind direction (WD; Figure 4c). At the multiday time scale, $CH_4$ flux only shared significant levels of information with ET and WD (Figure 4e). In total, 51.5% of total $CH_4$ flux variability occurred at the diel scale, 33.4% occurred the multiday scale, and 15.1% occurred at the hourly time scale (Figure 4a,c,e). Peat wetland $CH_4$ fluxes peaked between 10:00 and 12:00 local time (LT) coinciding with the period of peak NEE (Figure S1).

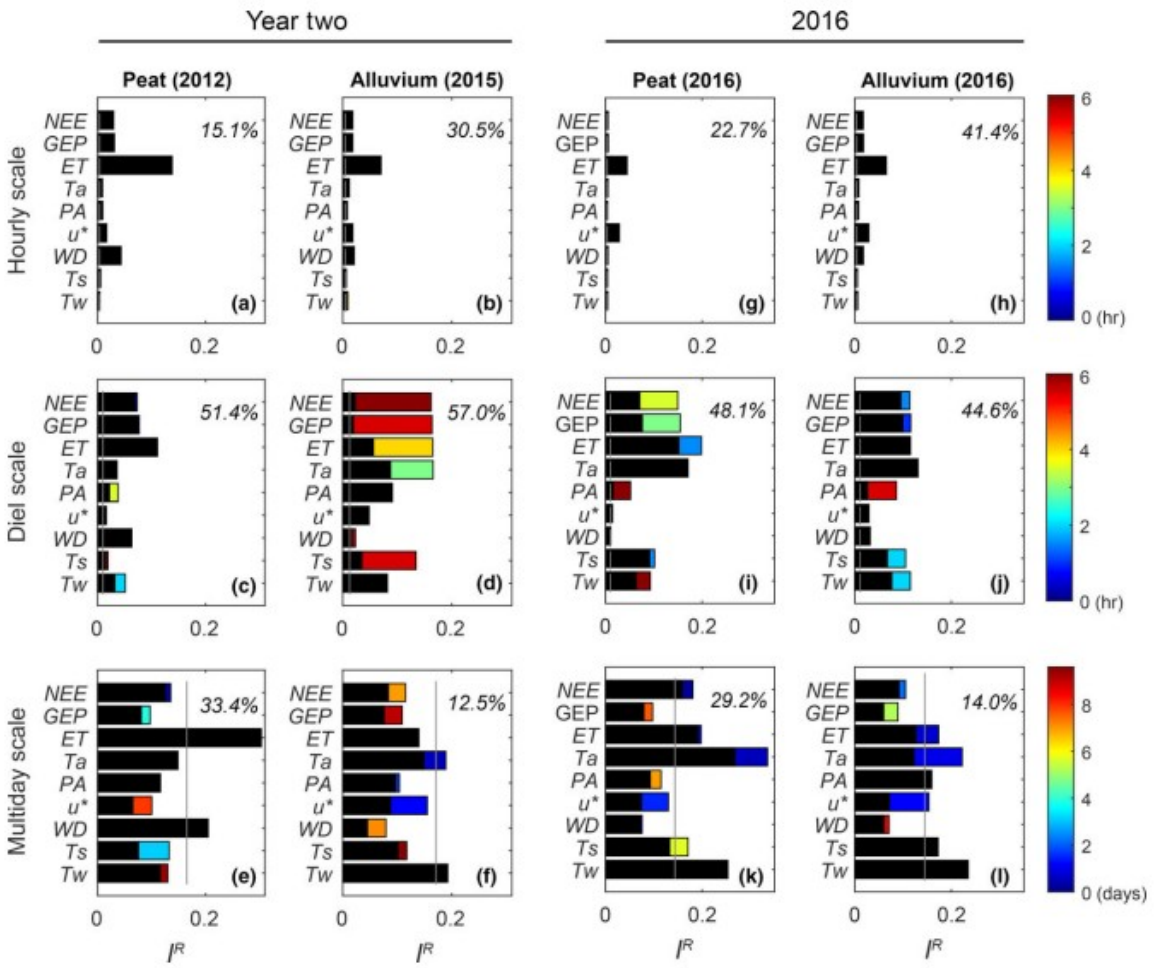


**FIGURE 4** Mutual information ($I^R$) shared between methane flux ($F_{CH4}$) and biophysical variables at multiple time scales for the peat and alluvium wetland (a–f) the second-year postrestoration (year 2) when both wetlands were fully vegetated and (g–l) during the 2016 growing season. Black bars indicate $I^R$ at zero time lag, and colored extension indicates maximum $I^R$ observed at the time lag illustrated by the color scale. Vertical gray bars represent 95% confidence intervals generated from 1,000 Monte Carlo random walks. Italicized percentage inset on each panel indicates the percent of total wavelet variance occurring at each time scale. Biophysical variables include net ecosystem exchange (NEE), gross ecosystem photosynthesis (GEP), evapotranspiration (ET), air temperature ($T_a$), air pressure (PA), friction velocity ($u^*$), wind direction (WD), soil temperature ($T_s$), and water temperature ($T_w$)

Alluvium wetland $CH_4$ flux patterns and interactions the second-year postrestoration (2015) were notably different from the peat wetland. Alluvium wetland $CH_4$ fluxes were dominantly coupled to physical processes at diel to multiday time scales, such as temperature and atmospheric pressure (PA) fluctuations (Figure 4b,d,f), in contrast to the peat site where fluxes were primarily coupled to plant processes (Figure 4a,c,e). At the hourly scale, $CH_4$ fluxes also shared most information with ET (Figure 4b). At the diel scale, dominant interactions were observed with PA and water temperature ($T_w$) at no time lag and with $T_a$ at a 3 hr lag (Figure 4d). Here, wetland maximum $CH_4$ fluxes were observed in the late afternoon during atmospheric pressure lows (17:00 to 19:00 LT), and this relationship displayed strong hysteresis (Figure S2). This dominant diel PA interaction was not observed at the peat site (Figure 4c). Strong interactions were also observed between $CH_4$ flux and GEP/NEE/ET, but these interactions occurred

at a 4–5 hr time lag (Figure 4d). These interactions can be intuitively seen through the timing of fluxes, where peak NEE and ET were observed mid-day, while peak $CH_4$ flux occurred many hours later in the afternoon (Figure S1). At the multiday scale, alluvium $CH_4$ fluxes only shared significant information with temperature variables ($T_a$ and $T_w$; Figure 4f). Hourly scale $CH_4$ flux variability was more dominant at the alluvium wetland in year 2, as 57.0% of total $CH_4$ flux signal variability occurred at the diel scale, 30.5% occurred at the hourly scale, and only 12.5% occurred at the multiday time scale (Figure 4b,d,f).

By the 2016 growing season, $CH_4$ flux patterns and interactions had converged across the peat and alluvium wetland sites. Peak $CH_4$ fluxes were observed at roughly 15:00 LT at both sites by 2016. This shift to an afternoon peak flux occurred in 2013 at the peat wetland, and patterns in flux timing were similar for each year thereafter (Figure S1). Both alluvium and peat sites were quite different in terms of flux timing compared with the mature site, where peak $CH_4$ flux occurred around noon most years (Figure S1).

Scale-emergent controls of $CH_4$ flux were also very similar between the alluvium and peat site during the 2016 growing season (Figure 4). For both sites, hourly $CH_4$ fluxes exhibited dominant synchronous couplings to friction velocity ($u^*$) and ET (Figure 4g,h), and at the diel scale, dominant interactions with $CH_4$ flux included $T_a$, ET, GEP, and NEE at both wetlands (Figure 4i,j). By 2016, dominant synchronous PA interactions observed at the alluvium site (Figure 4d) were no longer apparent, though PA shared similar levels of information with $CH_4$ flux at a 5–6 hr time lag (Figure 4j). Multiday scale interactions were also similar across sites, where significant interactions with temperature variables ($T_a$, $T_w$, and $T_s$), as well as ET, were observed (Figure 4k,l). There were some notable differences between sites at the multiday scale, as $CH_4$ flux also shared information with NEE at the peat site (Figure 4k), and $CH_4$ flux shared information with PA at the alluvium site (Figure 4l). At the peat wetland, most variability still occurred at the diel scale (48.1%), followed by the multiday (29.2%) and hourly (22.7%) time scales (Figure 4g,i,k). Most variability at the alluvium wetland still occurred at the diel scale (44.6%), followed closely by the hourly scale (41.4%), and much less variability occurred at the multiday scale (14.0%; Figure 4h,j,l).

### 3.4 What explains increasing alluvium $CH_4$ fluxes with time?

To determine whether long-term increases in alluvium wetland $CH_4$ emissions could be explained by common biophysical drivers, we trained an empirical $CH_4$ flux model using observations from a third independent, mature wetland site that was restored in 1999 and is located ~700 m from the alluvium wetland. The model predicted $CH_4$ fluxes based on nine common biophysical drivers identified here and in Sturtevant et al. (2016), including PAR, $T_a$, PA, $u^*$, GEP, ER, ET, a greenness index (GCC), and vapor pressure deficit. We fit a GAM using penalized regression splines to capture nonlinear relationships, and the model was fit to 4 years of daily flux data from the mature wetland

($n$ = 1,464), where tenfold cross-validation was used to tune the model for best fit (final model - no feature selection; $r^2$ = .78).

The trained GAM performed relatively well against observed peat wetland $CH_4$ fluxes ($r^2$ = .60). Within each year (2012–2017), residual $CH_4$ fluxes were distributed around zero and skewed slightly negative, indicating some overestimation in predicted fluxes. The model residual interquartile range (IQR) always overlapped with zero, except for 2017 when multiple disturbance events reduced CO2 and CH4 fluxes from the peat wetland (Figure 5).

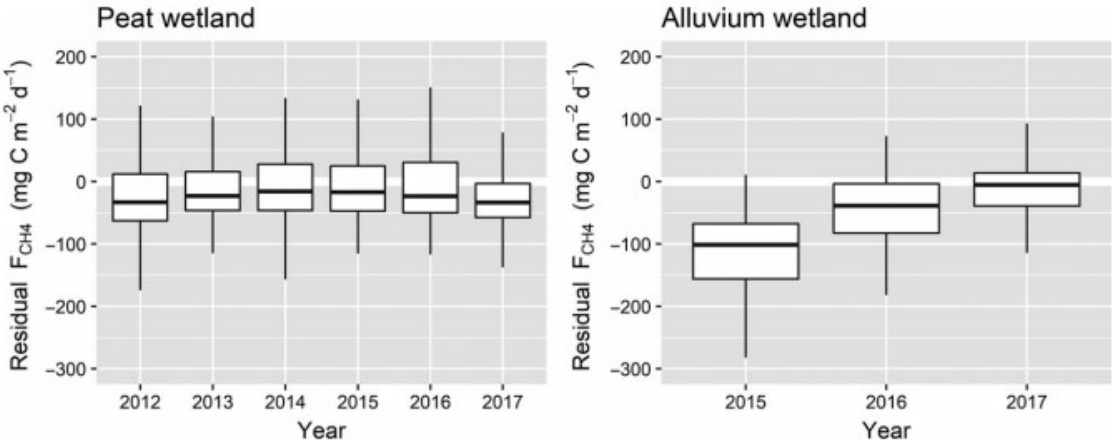


**FIGURE 5** Residual $CH_4$ flux ($F_{CH4}$; mg C $m^{-2}$ $day^{-1}$) for both recently restored wetlands using an empirical model trained on $CH_4$ fluxes from a mature, stable state wetland site restored in 1999. A generalized additive model was trained on 4 years of daily $CH_4$ fluxes using nine common biophysical drivers (see Results for details) and tenfold cross-validation. First-year fluxes were omitted from residual analysis because the model was trained on a fully vegetated, mature wetland

The GAM performance against the alluvium wetland was notably worse ($r^2$ = .34) and was highly variable across years (Figure 5). Observed alluvium $CH_4$ fluxes were substantially lower than model predictions the second year following restoration (2015), as indicated by negative residuals when the IQR did not cross zero (Figure 5). This strong negative skew reduced in subsequent years, and by 2017, there was no observed bias in model $CH_4$ residuals (Figure 5). The GAM predicted 72.6% of observed variance in 2017, indicating more accurate $CH_4$ flux predictions as the alluvium wetland developed.

Model over-prediction in early years at the alluvium wetland suggests that other factors, not measured directly by the eddy covariance tower, could have inhibited initial $CH_4$ emissions. Though our soil data was collected during a single sampling in 2017, we can substitute depth for time to track changes in soil properties over this time period. If we assume the parent horizon is indicative of soils at the time of restoration and the accreted horizon is indicative of the current state of wetland soils, we observe a significant increase in soil pH (Figure 2d) and a shift toward more Fe in its reduced form ($Fe^{2+}$) as alluvium wetland soils developed (Figure 2b).

### 3.5 Implications for restored wetland GHG emissions

Methane emissions from the alluvium wetland increased steadily with time. This stands in contrast to the trend of reducing $CH_4$ emissions in recent years at the other wetlands, where annual $CH_4$ budgets from the peat and mature wetland covaried and were not statistically different from one another from 2014 to 2017 (Figure 6a). By 2017, annual $CH_4$ fluxes from the alluvium wetland exceeded emissions from the peat and mature wetlands, although were significantly lower than emissions from the other sites in the previous 2 years (2015 and 2016; Figure 6a). In 2015, alluvium $CH_4$ budgets were 48%–50% the magnitude of the other sites, and in 2016, the alluvium $CH_4$ budget was 75%–78% of the other sites (Figure 6a). Reduced $CH_4$ budgets in 2015 and 2016 initially corresponded to neutral GHG emissions from the alluvium wetland (Figure 6b); however, by 2017, the alluvium GHG budget was positive and trended larger than the other sites (Figure 6b). Conversely, the peat and mature wetlands were both GHG sources from 2014 to 2016 and GHG neutral in 2017 (Figure 6b). Soil iron content (extractable and poorly crystalline Fe) was similar across parent horizons of peat and mature wetlands (Tukey's HSD, $p > .5$; Figure S5), although soil C concentrations were significantly higher at the mature wetland compared with the peat and alluvium sites (Tukey's HSD, $p < .01$; Figure S5). These wetlands experienced similar climatic and hydrologic conditions over this time period (Figure S3).

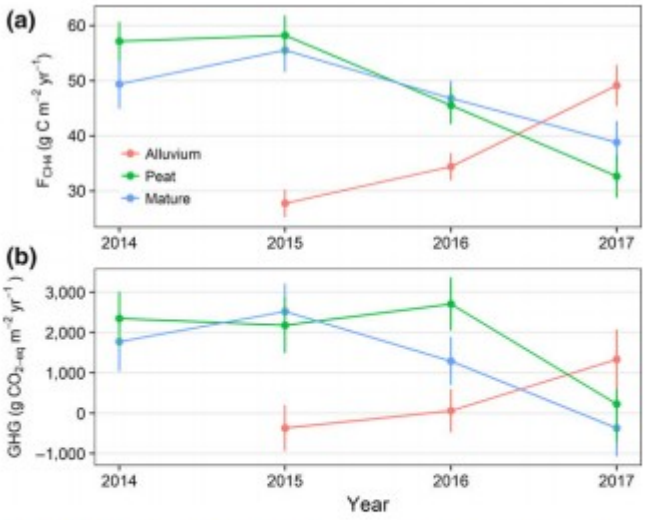


**FIGURE 6** Annual $CH_4$ flux ($F_{CH4}$) and greenhouse gas budgets (GHG) across the two recently restored peat and alluvium wetlands, as well as the mature wetland restored on peat soils. Annual GHG budget is computed from annual $F_{CH4}$ and NEE budgets using the sustained global warming potential for $CH_4$ (Neubauer & Megonigal, 2015)

## 4 DISCUSSION

Our results suggest that soil type, a legacy of the predrainage landscape, influences ecosystem-scale $CH_4$ emissions from restored wetlands. We observed substantially lower $CH_4$ emissions for multiple years following restoration from a wetland restored on alluvium compared with peat soils; however, $CH_4$ flux magnitudes converged across the wetlands 3 years postrestoration (Figure 3a). Initial $CH_4$ flux differences were not driven by variable climate or hydrologic forcing, as these wetlands experienced similar meteorologic conditions and both remained inundated year-round (Figure 3). In addition, alluvium NEE was often similar to, or larger than, NEE from the peat site (Figure 3b), demonstrating that differences in $CH_4$ flux were not due to covariation with other factors broadly affecting wetland GHG exchange. Soil Fe, C content, and pH are edaphic factors known to influence $CH_4$ production rates in soil (Bridgham et al., 2013; Teh et al., 2008; Ye et al., 2012). Soil C has been shown to be a strong proxy for $CH_4$ emissions from rewetted peatlands on these islands (Ye et al., 2016); however, soil C did not vary between wetlands at the time of restoration, as we observed similar C concentrations in parent horizons across both sites (Figure 2). In addition, soil C does not appear to drive $CH_4$ emissions more broadly across the wetland network, as annual $CH_4$ fluxes did not vary across peat and mature wetlands (Figure 6), though their soil C concentrations varied substantially (Figure S5). These observations suggest that reduced $CH_4$ emissions may instead be related to the acidic conditions and high Fe content in alluvium soils (Figure 2).

Alluvium soil Fe concentrations were comparable to tropical forest soils where microbial Fe reduction is known to inhibit $CH_4$ production. Yang and Liptzin (2015) observed mean Fe concentrations of 23.6 mg Fe/g soil in forest soils where Teh et al. (2008) had previously documented suppression of methanogenesis by microbial Fe reduction. Alluvium wetland Fe concentrations were similar (21.76 ± 5.88 mg Fe/g soil; $n = 30$), demonstrating that Fe concentrations were within the range where microbial Fe reduction inhibits methanogenesis. In contrast to upland humid tropical forests where most Fe is found in poorly crystalline form (Dubinsky et al., 2010; Hall & Silver, 2015; Yang & Liptzin, 2015), poorly crystalline Fe concentrations were roughly two orders of magnitude lower than the HCl-extractable Fe pool across the wetland sites. Poorly crystalline Fe pools are readily reducible by soil microbes (Hall & Silver, 2015; Hyacinthe et al., 2006), and depletion of these pools suggests high activity by microbial Fe reducers in wetland soils (Weiss, Emerson, & Megonigal, 2004). Depleted reducible Fe pools in wetlands relative to upland systems is expected, as stable anoxic wetland conditions promotes extended Fe reducer activity and utilization of poorly crystalline Fe pools (Dubinsky et al., 2010; Teh et al., 2008). Our observations of high Fe concentrations, low poorly crystalline Fe pools, and low $CH_4$ fluxes at the alluvium wetland all suggest that Fe reduction is a dominant form of anaerobic respiration capable of inhibiting $CH_4$ flux at this site. Differences in soil pH may also contribute to observed

flux differences; however, strong inhibition of methanogenesis tends to occur at pH values below 5 (Dunfield, Knowles, Dumont, & Moore, 1993; Kotsyurbenko et al., 2007; Ye et al., 2012), while we observed mean pH values of 5.27 in the alluvium parent soils. Further incubation experiments are warranted to disentangle the direct mechanism reducing $CH_4$ fluxes, as pH, Fe cycling, and redox state co-vary in inundated soils (Gotoh & Patrick, 1974).

The question remains: Why did $CH_4$ flux differences between the peat and alluvium wetlands disappear with time? Our empirical model based on dominant biophysical drivers of mature wetland $CH_4$ flux, including NEE, GEP, and ER, could not explain why alluvium $CH_4$ fluxes were initially low relative to the other sites (Figure 6), suggesting that other factors might be responsible for reduced fluxes in early succession. We suspect this is related to soil development over time, as we observed increases in reduced ferrous iron ($Fe^{2+}$) and a shift toward less acidic conditions in alluvium accreted soil compared with the underlying parent soil (Figure 2). Increases in $Fe^{2+}$ and pH suggest more reduced conditions favorable to methanogenesis in the accreted soils where poorly crystalline Fe pools are depleted faster than they are replenished. Acidic soils are also known to directly inhibit methanogenesis (Dunfield et al., 1993; Ye et al., 2012) and alter methanogen community structure (Kotsyurbenko et al., 2007), although often in more acidic conditions as described above. This interaction between less acidic and more reduced conditions could enhance $CH_4$ production rates in the newly accreted soils as alluvium wetlands develop.

Initial differences in wetland biophysical $CH_4$ drivers the second year following restoration provide a further line of evidence that alluvium $CH_4$ fluxes were inhibited by Fe reduction. Alluvium $CH_4$ fluxes were decoupled from plant processes across multiple scales compared with the peat site. Peat $CH_4$ fluxes were more dominantly coupled to plant processes, such as GEP and ET (Figure 4), while alluvium $CH_4$ fluxes were more dominantly coupled to physical transport (pressure pumping; Figure S2) and temperature, which dictates $CH_4$ production rates in bulk soil (Yvon-Durocher et al., 2014). This decoupling from plant-derived substrates (GEP) and transport pathways (ET) suggests that less $CH_4$ was derived from plant exudates in the rhizosphere. Oxygen is released into wetland soils through plant roots, and the rhizosphere is typically an area of high $CH_4$ oxidation (Laanbroek, 2010; van der Nat & Middelburg, 1998). The wetland rhizosphere is also a hotspot of microbial Fe oxidation and reduction given the co-occurrence of oxic-anoxic conditions (Weiss, Emerson, Backer, & Megonigal, 2003). For sites with higher Fe, such as the alluvium wetland, $CH_4$ fluxes might be more decoupled from plant substrates (GEP) and transport pathways (ET) where rhizosphere methanogenesis is further inhibited by active Fe redox cycling (Laanbroek, 2010). Such inhibition of methanogenesis has been observed in microcosm and incubation studies, where oxygen input via plant roots re-oxidizes ferrous Fe and further

suppresses $CH_4$ production in the root zone (Frenzel, Bosse, & Janssen, 1999; Roden & Wetzel, 1996; Sutton-Grier & Megonigal, 2011). Anaerobic microbial re-oxidation of Fe coupled to $NO_3^-$ reduction is also known to occur in wetland sediments (Weber, Urrutia, Churchill, Kukkadapu, & Roden, 2006) and may be relevant to Fe cycling in these wetlands if significant $NO_3^-$ enters the system from upslope agriculture.

Conversely, we might expect to see stronger couplings to plant processes for sites with lower soil Fe concentrations, as we observe for the peat wetland (Figure 4). Sturtevant et al. (2016) also demonstrated strong diel $CH_4$ couplings to ET and GEP at the mature wetland where soil Fe concentrations are low relative to the alluvium site (Figure S5). Hatala, Detto, Baldocchi (2012) and Knox et al. (2016) found that diel patterns in $CH_4$ fluxes from Delta rice were driven by *GEP*, rather than temperature, because peak $CH_4$ flux lagged *GEP* by ~1–2 hr and led maximum soil temperature. We saw a very different dynamic at the alluvium wetland where peak $CH_4$ flux occurred late in the afternoon, many hours after peak GEP, ET, and $T_a$, and was instead synchronously coupled to PA and $T_w$ fluctuations (Figure 4). These dynamics further suggest decoupling from recent plant-derived C substrates and transport pathways at the alluvium wetland, with more dominant couplings to physical transport and drivers of bulk soil methanogenesis, as expected if rhizosphere $CH_4$ production was inhibited by active Fe redox.

Convergence of $CH_4$ flux biophysical drivers with time further suggests that as soils develop $CH_4$ fluxes and controls become more similar across wetland types. The hierarchy of dominant biophysical drivers and lagged effects were quite similar across the peat and alluvium wetlands in 2016 (Figure 4g–l) compared with the second year when flux-driver relationships were very different across the two systems (Figure 4a–f). Here, the most notable shift occurred at the alluvium wetland, where $CH_4$ fluxes were strongly coupled to physical processes in the second year (Figure 4b,d,f), and by 2016, fluxes were also coupled to plant processes across multiple scales, such as NEE, GEP, and ET (Figure 4h,j,l). The mature wetland GAM was also better able to predict alluvium wetland $CH_4$ fluxes as this shift occurred (Figure 5), further suggesting stronger couplings to plant processes as the alluvium wetland and its soils developed.

Differences in controls across scale are discussed in more detail in Sturtevant et al. (2016), but we find short-term (hourly) variability in $CH_4$ flux is influenced by transport mechanisms (ET and $u^*$), diel variation is more dictated by plant processes and temperature (NEE, GEP, ET, and $T_a$), while weekly to monthly variation is driven by temperature oscillations. Surprisingly, much more flux variability occurred at the multiday scale for the peat wetland than the alluvium wetland, and this pattern was consistent over time (Figure 4). While the driver of this inter-site variation is not clear, it demonstrates that eddy covariance is particularly well-suited to ecosystem $CH_4$ flux measurements. Nonautomated chamber measurement campaigns

could easily under-sample important modes of $CH_4$ flux variation, particularly if dominant modes of variation change across wetlands distributed over small spatial scales.

Overall, our findings demonstrate that soil type impacts ecosystem-scale $CH_4$ emissions and GHG budgets from restored wetlands on annual time scales. We found that differences in $CH_4$ flux between alluvium and peat wetlands were pronounced for the first few years following restoration, causing significant reductions in net GHG emissions from the wetland restored on alluvium soils (Figure 6). Initial differences were most likely due to high Fe content within alluvium soils, as Fe concentrations were in the range where inhibition of methanogenesis is known to occur (Teh et al., 2008), and soil C, another common driver of $CH_4$ emissions (Ye et al., 2016), did not vary across sites at the initial point of restoration. However, reduced $CH_4$ emissions and GHG budgets faded with time, likely due to the development of more reduced, less acidic conditions favorable to $CH_4$ production within accreted alluvium sediments. Wetland restoration projects have a lifetime of multiple decades (over 20 years for the mature wetland), so these transient reductions in $CH_4$ flux are likely of low importance from a policy or management perspective because any GHG benefit of restoring wetlands on alluvium soil are lost within a few years of restoration. This work illustrates a transient influence of soil properties on long-term wetland GHG emissions, which improves our understanding of site selection consequences to GHG emissions from restored wetlands.

ACKNOWLEDGEMENTS

This research was supported, in part, by the U.S. Department of Energy's Office of Science and its funding of Ameriflux core sites (Ameriflux contract 7079856), and the California Division of Fish and Wildlife, through a Contract of the California Department of Water Resources (award 4600011240). We thank three anonymous reviewers for their constructive feedback on drafts of this manuscript.

References

Ali, M. A., Lee, C. H., Lee, Y. B., & Kim, P. J. (2009). Silicate fertilization in no-tillage rice farming for mitigation of methane emission and increasing rice productivity. *Agriculture, Ecosystems & Environment*, 132, 16–22.https://doi.org/10.1016/j.agee.2009.02.014

Angle, J. C., Morin, T. H., Solden, L. M., Narrowe, A. B., Smith, G. J., Borton, M. A., … Wrighton, K. C. (2017). Methanogenesis in oxygenated soils is a substantial fraction of wetland methane emissions. *Nature Communications*, 8, 1567. https://doi.org/10.1038/s41467-017-01753-4

Atwater, B. F., & Belknap, D. F. (1980). Tidal-wetland deposits of the Sacramento-San Joaquin Delta, California. In M. E. Field, A. H. Bouma, I. P. Coburn, R. G. Douglas, & J. C. Ingle (Eds.), *Quaternary depositional environments of the Pacific Coast: Pacific Coast paleogeography symposium*

*4* (pp. 89– 103). Los Angeles, CA: The Pacific Section of the Society of Economic Paleontologists; Mineralogists.

Atwater, B. F., Conrad, S., Dowden, J. N., Hedel, C. W., MacDonald, R. L., & Savage, W. (1979). History, landforms, and vegetation of the estuary's tidal marshes. In T. J. Conomos (Ed.), *San Francisco Bay: The urbanized estuary: Investigations into the natural history of San Francisco Bay and Delta with reference to the influence of man* (pp. 347– 386). San Francisco, CA: AAAS Pacific Division.

Auguie, B. (2016). gridExtra: Miscellaneous functions for “grid” graphics. Retrieved from https://CRAN.R677project.org/package=gridExtra

Baldocchi, D., Sturtevant, C., & Fluxnet Contributors (2015). Does day and night sampling reduce spurious correlation between canopy photosynthesis and ecosystem respiration? *Agricultural and Forest Meteorology*, 207, 117–126. https://doi.org/10.1016/j.agrformet.2015.03.010

Bridgham, S. D., Cadillo-Quiroz, H., Keller, J. K., & Zhuang, Q. (2013). Methane emissions from wetlands: Biogeochemical, microbial, and modeling perspectives from local to global scales. *Global Change Biology*, 19, 1325–1346. https://doi.org/10.1111/gcb.12131

Brown, M. G., Humphreys, E. R., Moore, T. R., Roulet, N. T., & Lafleur, P. M. (2014). Evidence for a nonmonotonic relationship between ecosystem-scale peatland methane emissions and water table depth. *Journal of Geophysical Research: Biogeosciences*, 119, 826– 835.

Bubier, J. L., & Moore, T. R. (1994). An ecological perspective on methane emissions from northern wetlands. *Trends in Ecology & Evolution*, 9, 460–464. https://doi.org/10.1016/0169-5347(94)90309-3

Chamberlain, S. D., Boughton, E. H., & Sparks, J. P. (2015). Underlying ecosystem emissions exceed cattle-emitted methane from subtropical lowland pastures. *Ecosystems*, 18, 933– 945. https://doi.org/10.1007/s10021-015-9873-x

Chamberlain, S. D., Gomez-Casanovas, N., Walter, M. T., Boughton, E. H., Bernacchi, C. J., DeLucia, E. H., … Sparks, J. P. (2016). Influence of transient flooding on methane fluxes from subtropical pastures. *Journal of Geophysical Research: Biogeosciences*, 121, 965– 977.

Chamberlain, S. D., Groffman, P. M., Boughton, E. H., Gomez-Casanovas, N., DeLucia, E. H., Bernacchi, C. J., & Sparks, J. P. (2017). The impact of water management practices on subtropical pasture methane emissions and ecosystem service payments. *Ecological Applications*, 27, 1199– 1209. https://doi.org/10.1002/eap.1514

Chamberlain, S. D., Verfaillie, J., Eichelmann, E., Hemes, K. S., & Baldocchi, D. D. (2017). Evaluation of density corrections to methane fluxes measured by open-path eddy covariance over contrasting landscapes. *Boundary-Layer Meteorology*, 165, 197– 210. https://doi.org/10.1007/s10546-017-0275-9

Chu, H., Chen, J., Gottgens, J. F., Ouyang, Z., John, R., Czajkowski, K., & Becker, R. (2014). Net ecosystem methane and carbon dioxide exchanges in a Lake Erie coastal marsh and a nearby cropland. *Journal of Geophysical Research: Biogeosciences*, 119, 722– 740.

Conrad, R. (2009). The global methane cycle: Recent advances in understanding the microbial processes involved. *Environmental Microbiology Reports*, 1, 285– 292. https://doi.org/10.1111/j.1758-2229.2009.00038.x

Conservation International (2017). The Blue Carbon Initiative. Retrieved from http://thebluecarboninitiative.org/

Detto, M., Montaldo, N., Albertson, J. D., Mancini, M., & Katul, G. (2006). Soil moisture and vegetation controls on evapotranspiration in a heterogeneous Mediterranean ecosystem on Sardinia, Italy. *Water Resources Research*, 42, W08419.

Deverel, S. J., & Leighton, D. A. (2010). Historic, recent, and future subsidence, Sacramento-San Joaquin Delta, California, USA. *San Francisco Estuary and Watershed Science*, 8, 1– 23.

Drexler, J. Z. (2011). Peat formation processes through the millennia in tidal marshes of the Sacramento-San Joaquin Delta, California, USA. *Estuaries and Coasts*, 34, 900– 911. https://doi.org/10.1007/s12237-011-9393-7

Drexler, J. Z., de Fontaine, C. S., & Brown, T. A. (2009). Peat accretion histories during the past 6,000 years in marshes of the Sacramento-San Joaquin Delta, CA, USA. *Estuaries and Coasts*, 32, 871– 892. https://doi.org/10.1007/s12237-009-9202-8

Dubinsky, E. A., Silver, W. L., & Firestone, M. K. (2010). Tropical forest soil microbial communities couple iron and carbon biogeochemistry. *Ecology*, 91, 2604– 2612. https://doi.org/10.1890/09-1365.1

Dunfield, P., Knowles, R., Dumont, R., & Moore, T. R. (1993). Methane production and consumption in temperate and subarctic peat soils: Response to temperature and pH. *Soil Biology and Biochemistry*, 25, 321– 326. https://doi.org/10.1016/0038-0717(93)90130-4

Eichelmann, E., Hemes, K. S., Knox, S. H., Oikawa, P. Y., Chamberlain, S. D., Sturtevant, C., … Baldocchi, D. D. (2018). The effect of land cover type and stand structure on evapotranspiration from agricultural and wetland sites in the Sacramento-San Joaquin River Delta, California. *Agricultural and Forest Meteorology*, 256– 257, 179–195. https://doi.org/10.1016/j.agrformet.2018.03.007

Forbrich, I., Kutzbach, L., Wille, C., Becker, T., Wu, J., & Wilmking, M. (2011). Cross-evaluation of measurements of peatland methane emissions on microform and ecosystem scales using high-resolution landcover classification and source weight modelling. *Agricultural and Forest Meteorology*, 151, 864– 874. https://doi.org/10.1016/j.agrformet.2011.02.006

Frenzel, P., Bosse, U., & Janssen, P. H. (1999). Rice roots and methanogenesis in a paddy soil: Ferric iron as an alternative electron acceptor in the rooted soil. *Soil Biology and Biochemistry*, 31, 421– 430. https://doi.org/10.1016/S0038-0717(98)00144-8

Goodrich, J. P., Campbell, D. I., Roulet, N. T., Clearwater, M. J., & Schipper, L. A. (2015). Overriding control of methane flux temporal variability by water table dynamics in a southern hemisphere, raised bog. *Journal of Geophysical Research: Biogeosciences*, 120, 819– 831.

Gotoh, S., & Patrick, W. H. (1974). Transformation of iron in a waterlogged soil as influenced by redox potential and pH 1. *Soil Science Society of America Journal*, 38, 66– 71. https://doi.org/10.2136/sssaj1974.03615995003800010024x

Graham, R., & O'Geen, A. (2010). Soil mineralogy trends in California landscapes. *Geoderma*, 154, 418– 437. https://doi.org/10.1016/j.geoderma.2009.05.018

Grolemund, G., & Wickham, H. (2011). Dates and times made easy with lubridate. *Journal of Statistical Software*, 40, 1– 25.

Hall, S. J., & Silver, W. L. (2013). Iron oxidation stimulates organic matter decomposition in humid tropical forest soils. *Global Change Biology*, 19, 2804– 2813. https://doi.org/10.1111/gcb.12229

Hall, S. J., & Silver, W. L. (2015). Reducing conditions, reactive metals, and their interactions can explain spatial patterns of surface soil carbon in a humid tropical forest. *Biogeochemistry*, 125, 149– 165. https://doi.org/10.1007/s10533-015-0120-5

Hansson, L.-A., Brönmark, C., Anders Nilsson, P., & Åbjörnsson, K. (2005). Conflicting demands on wetland ecosystem services: Nutrient retention, biodiversity or both? *Freshwater Biology*, 50, 705– 714. https://doi.org/10.1111/j.1365-2427.2005.01352.x

Hatala, J. A., Detto, M., & Baldocchi, D. D. (2012). Gross ecosystem photosynthesis causes a diurnal pattern in methane emission from rice. *Geophysical Research Letters*, 39, L06409.

Hatala, J. A., Detto, M., Sonnentag, O., Deverel, S. J., Verfaillie, J., & Baldocchi, D. D. (2012). Greenhouse gas ($CO_2$, $CH_4$, $H_2O$) fluxes from drained and flooded agricultural peatlands in the Sacramento-San Joaquin Delta. *Agriculture, Ecosystems & Environment*, 150, 1– 18. https://doi.org/10.1016/j.agee.2012.01.009

Hendriks, D. M. D., van Huissteden, J., & Dolman, A. J. (2010). Multi-technique assessment of spatial and temporal variability of methane fluxes in a peat meadow. *Agricultural and Forest Meteorology*, 150, 757– 774. https://doi.org/10.1016/j.agrformet.2009.06.017

Hendriks, D. M. D., van Huissteden, J., Dolman, A. J., & van der Molen, M. K. (2007). The full greenhouse gas balance of an abandoned peat meadow. *Biogeosciences*, 4, 411– 424. https://doi.org/10.5194/bg-4-411-2007

Holm, G. O., Perez, B. C., McWhorter, D. E., Krauss, K. W., Johnson, D. J., Raynie, R. C., & Killebrew, C. J. (2016). Ecosystem level methane fluxes from tidal freshwater and brackish marshes of the Mississippi River Delta: Implications for coastal wetland carbon projects. *Wetlands*, 36, 401– 413. https://doi.org/10.1007/s13157-016-0746-7

Hsieh, C.-I., Katul, G., & Chi, T.-w. (2000). An approximate analytical model for footprint estimation of scalar fluxes in thermally stratified atmospheric flows. *Advances in Water Resources*, 23, 765– 772. https://doi.org/10.1016/S0309-1708(99)00042-1

Hyacinthe, C., Bonneville, S., & Van Cappellen, P. (2006). Reactive iron(III) in sediments: Chemical versus microbial extractions. *Geochimica et Cosmochimica Acta*, 70, 4166– 4180. https://doi.org/10.1016/j.gca.2006.05.018

Jäckel, U., & Schnell, S. (2000). Suppression of methane emission from rice paddies by ferric iron fertilization. *Soil Biology and Biochemistry*, 32, 1811– 1814. https://doi.org/10.1016/S0038-0717(00)00094-8

Kassambara, A. (2017). ggpubr: 'ggplot2' based publication ready plots. Retrieved from https://CRAN.R758project.org/package=ggpubr

Kirschke, S., Bousquet, P., Ciais, P., Saunois, M., Canadell, J. G., Dlugokencky, E. J., … Cameron-Smith, P. (2013). Three decades of global methane sources and sinks. *Nature Geoscience*, 6, 813– 823. https://doi.org/10.1038/ngeo1955

Knox, S. H., Matthes, J. H., Sturtevant, C., Oikawa, P. Y., Verfaillie, J., & Baldocchi, D. (2016). Biophysical controls on interannual variability in ecosystem-scale $CO_2$ and $CH_4$ exchange in a California rice paddy. *Journal of Geophysical Research: Biogeosciences*, 121, 978– 1001.

Knox, S. H., Sturtevant, C., Matthes, J. H., Koteen, L., Verfaillie, J., & Baldocchi, D. (2015). Agricultural peatland restoration: Effects of land-use change on greenhouse gas ($CO_2$ and $CH_4$) fluxes in the Sacramento-San Joaquin Delta. *Global Change Biology*, 21, 750– 765. https://doi.org/10.1111/gcb.12745

Kotsyurbenko, O. R., Friedrich, M. W., Simankova, M. V., Nozhevnikova, A. N., Golyshin, P. N., Timmis, K. N., & Conrad, R. (2007). Shift from acetoclastic to $H_2$-dependent methanogenesis in a West Siberian peat bog at low pH values and isolation of an acidophilic methanobacterium strain. *Applied and Environmental Microbiology*, 73, 2344– 2348. https://doi.org/10.1128/AEM.02413-06

Krauss, K. W., Holm, G. O., Perez, B. C., McWhorter, D. E., Cormier, N., Moss, R. F., … Raynie, R. C. (2016). Component greenhouse gas fluxes and radiative balance from two deltaic marshes in Louisiana: Pairing chamber

techniques and eddy covariance. *Journal of Geophysical Research: Biogeosciences*, 121, 1503– 1521.

Kuhn, M. (2017). caret: Classification and regression training. Retrieved from https://CRAN.R-project.org/package=caret

Laanbroek, H. J. (2010). Methane emission from natural wetlands: Interplay between emergent macrophytes and soil microbial processes. a mini-review. *Annals of Botany*, 105, 141– 153. https://doi.org/10.1093/aob/mcp201

Lal, R. (2008). Carbon sequestration. *Philosophical Transactions of the Royal Society B: Biological Sciences*, 363, 815– 830. https://doi.org/10.1098/rstb.2007.2185

Levy, P. E., Burden, A., Cooper, M. D., Dinsmore, K. J., Drewer, J., Evans, C., … Jones, T. (2012). Methane emissions from soils: Synthesis and analysis of a large UK data set. *Global Change Biology*, 18, 1657– 1669. https://doi.org/10.1111/j.1365-2486.2011.02616.x

Matthes, J. H., Sturtevant, C., Verfaillie, J., Knox, S., & Baldocchi, D. (2014). Parsing the variability in $CH_4$ flux at a spatially heterogeneous wetland: Integrating multiple eddy covariance towers with high-resolution flux footprint analysis. *Journal of Geophysical Research: Biogeosciences*, 119, 1322– 1339.

McNicol, G., Sturtevant, C. S., Knox, S. H., Dronova, I., Baldocchi, D. D., & Silver, W. L. (2017). Effects of seasonality, transport pathway, and spatial structure on greenhouse gas fluxes in a restored wetland. *Global Change Biology*, 23, 2768– 2782. https://doi.org/10.1111/gcb.13580

Miller, R. L. (2011). Carbon gas fluxes in re-established wetlands on organic soils differ relative to plant community and hydrology. *Wetlands*, 31, 1055– 1066. https://doi.org/10.1007/s13157-011-0215-2

Miller, R. L., Fram, M., Fujii, R., & Wheeler, G. (2008). Subsidence reversal in a re-established wetland in the Sacramento-San Joaquin Delta, California, USA. *San Francisco Estuary and Watershed Science*, 6, 1– 20.

Miller, K. E., Lai, C.-T., Friedman, E. S., Angenent, L. T., & Lipson, D. A. (2015). Methane suppression by iron and humic acids in soils of the Arctic Coastal Plain. *Soil Biology and Biochemistry*, 83, 176– 183. https://doi.org/10.1016/j.soilbio.2015.01.022

Mitsch, W. J., Bernal, B., Nahlik, A. M., Mander, Ü., Zhang, L., Anderson, C. J., … Brix, H. (2013). Wetlands, carbon, and climate change. *Landscape Ecology*, 28, 583– 597. https://doi.org/10.1007/s10980-012-9758-8

Mitsch, W. J., Wu, X., Nairn, R. W., Weihe, P. E., Wang, N., Deal, R., & Boucher, C. E. (1998). Creating and restoring wetlands. *BioScience*, 48, 1019– 1030. https://doi.org/10.2307/1313458

Morin, T. H., Bohrer, G., Frasson, R. P. D. M., Naor-Azreli, L., Mesi, S., Stefanik, K. C., & Schäfer, K. V. R. (2014). Environmental drivers of methane

fluxes from an urban temperate wetland park. *Journal of Geophysical Research: Biogeosciences*, 119, 2188– 2208.

Morin, T. H., Bohrer, G., Stefanik, K. C., Rey-Sanchez, A. C., Matheny, A. M., & Mitsch, W. J. (2017). Combining eddy-covariance and chamber measurements to determine the methane budget from a small, heterogeneous urban floodplain wetland park. *Agricultural and Forest Meteorology*, 237–238, 160– 170. https://doi.org/10.1016/j.agrformet.2017.01.022

van der Nat, F.-J. W. A., & Middelburg, J. J. (1998). Seasonal variation in methane oxidation by the rhizosphere of *Phragmites australis* and *Scirpus lacustris*. *Aquatic Botany*, 61, 95– 110.

Neubauer, S. C., Givler, K., Valentine, S., & Megonigal, J. P. (2005). Seasonal patterns and plant-mediated controls of subsurface wetland biogeochemistry. *Ecology*, 86, 3334– 3344. https://doi.org/10.1890/04-1951

Neubauer, S. C., & Megonigal, J. P. (2015). Moving beyond global warming potentials to quantify the climatic role of ecosystems. *Ecosystems*, 18, 1000–1013.

Nisbet, E. G., Dlugokencky, E. J., Manning, M. R., Lowry, D., Fisher, R. E., France, J. L., … Bousquet, P. (2016). Rising atmospheric methane: 2007–2014 growth and isotopic shift. *Global Biogeochemical Cycles*, 30, 1356– 1370. https://doi.org/10.1002/2016GB005406

Oikawa, P. Y., Jenerette, G. D., Knox, S. H., Sturtevant, C., Verfaillie, J., Dronova, I., … Baldocchi, D. D. (2017). Evaluation of a hierarchy of models reveals importance of substrate limitation for predicting carbon dioxide and methane exchange in restored wetlands. *Journal of Geophysical Research: Biogeosciences*, 122, 145– 167.

Oikawa, P. Y., Sturtevant, C., Knox, S. H., Verfaillie, J., Huang, Y. W., & Baldocchi, D. D. (2017). Revisiting the partitioning of net ecosystem exchange of $CO_2$ into photosynthesis and respiration with simultaneous flux measurements of $^{13}CO_2$ and $CO_2$, soil respiration and a biophysical model, CANVEG. *Agricultural and Forest Meteorology*, 234–235, 149– 163. https://doi.org/10.1016/j.agrformet.2016.12.016

Olson, D. M., Griffis, T. J., Noormets, A., Kolka, R., & Chen, J. (2013). Interannual, seasonal, and retrospective analysis of the methane and carbon dioxide budgets of a temperate peatland. *Journal of Geophysical Research: Biogeosciences*, 118, 226– 238.

Petrescu, A. M., Lohila, A., Tuovinen, J. P., Baldocchi, D. D., Desai, A. R., Roulet, N. T., … Friborg, T. (2015). The uncertain climate footprint of wetlands under human pressure. *Proceedings of the National Academy of Sciences of the United States of America*, 112, 4594– 4599. https://doi.org/10.1073/pnas.1416267112

Poffenbarger, H. J., Needelman, B. A., & Megonigal, J. P. (2011). Salinity influence on methane emissions from tidal marshes. *Wetlands*, 31, 831– 842. https://doi.org/10.1007/s13157-011-0197-0

R Core Team (2017). *R: A language and environment for statistical computing*. Vienna, Austria: R Foundation for Statistical Computing. Retrieved from https://www.R-project.org/

Rey-Sanchez, A. C., Morin, T. H., Stefanik, K. C., Wrighton, K., & Bohrer, G. (2017). Determining total emissions and environmental drivers of methane flux in a Lake Erie estuarine marsh. *Ecological Engineering*, https://doi.org/10.1016/j.ecoleng.2017.06.042

Rinne, J., Riutta, T., Pihlatie, M., Aurela, M., Haapanala, S., Tuovinen, J. P., ... Vesala, T. (2007). Annual cycle of methane emission from a boreal fen measured by the eddy covariance technique. *Tellus Series B*, 59, 449– 457. https://doi.org/10.1111/j.1600-0889.2007.00261.x

Roden, E. E., & Wetzel, R. G. (1996). Organic carbon oxidation and suppression of methane production by microbial Fe(III) oxide reduction in vegetated and unvegetated freshwater wetland sediments. *Limnology and Oceanography*, 41, 1733– 1748. https://doi.org/10.4319/lo.1996.41.8.1733

Ruddell, B. L., Brunsell, N. A., & Stoy, P. (2013). Applying information theory in the geosciences to quantify process uncertainty, feedback, scale. *Eos, Transactions American Geophysical Union*, 94, 56. https://doi.org/10.1002/2013EO050007

Saunois, M., Bousquet, P., Poulter, B., Peregon, A., Ciais, P., Canadell, J. G., ... Janssens-Maenhout, G. (2016). The global methane budget 2000–2012. *Earth System Science Data*, 8, 697– 751. https://doi.org/10.5194/essd-8-697-2016

Shannon, C. E., & Weaver, W. (1998). *The mathematical theory of communication*. Urbana, IL: University of Illinois Press.

Soil Survey Staff (2017). Web soil survey. USDA Natural Resources Conservation Service. Retrieved from https://websoilsurvey.sc.egov.usda.gov

Sturtevant, C., Ruddell, B. L., Knox, S. H., Verfaillie, J., Matthes, J. H., Oikawa, P. Y., & Baldocchi, D. (2016). Identifying scale-emergent, nonlinear, asynchronous processes of wetland methane exchange. *Journal of Geophysical Research: Biogeosciences*, 121, 188– 204.

Sutton-Grier, A. E., & Megonigal, J. P. (2011). Plant species traits regulate methane production in freshwater wetland soils. *Soil Biology and Biochemistry*, 43, 413– 420. https://doi.org/10.1016/j.soilbio.2010.11.009

Swain, H. M., Boughton, E. H., Bohlen, P. J., & Lollis, L. O. (2013). Trade-offs among ecosystem services and disservices on a Florida ranch. *Rangelands*, 35, 75– 87. https://doi.org/10.2111/RANGELANDS-D-13-00053.1

Teh, Y. A., Dubinsky, E. A., Silver, W. L., & Carlson, C. M. (2008). Suppression of methanogenesis by dissimilatory Fe(III)-reducing bacteria in tropical rain

forest soils: Implications for ecosystem methane flux. *Global Change Biology*, 14, 413– 422.

Turetsky, M. R., Kotowska, A., Bubier, J., Dise, N. B., Crill, P., Hornibrook, E. R., … Olefeldt, D. (2014). A synthesis of methane emissions from 71 northern, temperate, and subtropical wetlands. *Global Change Biology*, 20, 2183– 2197. https://doi.org/10.1111/gcb.12580

Viollier, E., Inglett, P. W., Hunter, K., Roychoudhury, A. N., & Van Cappellen, P. (2000). The ferrozine method revisited: Fe(II)/Fe(III) determination in natural waters. *Applied Geochemistry*, 15, 785– 790. https://doi.org/10.1016/S0883-2927(99)00097-9

Weber, K. A., Urrutia, M. M., Churchill, P. F., Kukkadapu, R. K., & Roden, E. E. (2006). Anaerobic redox cycling of iron by freshwater sediment microorganisms. *Environmental Microbiology*, 8, 100– 113. https://doi.org/10.1111/j.1462-2920.2005.00873.x

Weiss, J. V., Emerson, D., Backer, S. M., & Megonigal, J. P. (2003). Enumeration of Fe(II)-oxidizing and Fe(III)-reducing bacteria in the root zone of wetland plants: Implications for a rhizosphere iron cycle. *Biogeochemistry*, 64, 77– 96. https://doi.org/10.1023/A:1024953027726

Weiss, J. V., Emerson, D., & Megonigal, J. P. (2004). Geochemical control of microbial Fe(III) reduction potential in wetlands: Comparison of the rhizosphere to non-rhizosphere soil. *FEMS Microbiology Ecology*, 48, 89– 100.

Whalen, S. (2005). Biogeochemistry of methane exchange between natural wetlands and the atmosphere. *Environmental Engineering Science*, 22, 73–94. https://doi.org/10.1089/ees.2005.22.73

Whiting, G. J., & Chanton, J. P. (2001). Greenhouse carbon balance of wetlands: Methane emission versus carbon sequestration. *Tellus B: Chemical and Physical Meteorology*, 53, 521– 528.

Wickham, H. (2016). scales: Scale functions for visualization. Retrieved from https://CRAN.R870project.org/package=scales

Wickham, H. (2017). tidyverse: Easily install and load ‘tidyverse’ packages. Retrieved from https://CRAN.R872project.org/package=tidyverse

Wille, C., Kutzbach, L., Sachs, T., Wagner, D., & Pfeiffer, E.-M. (2008). Methane emission from Siberian Arctic polygonal tundra: Eddy covariance measurements and modeling. *Global Change Biology*, 14, 1395– 1408. https://doi.org/10.1111/j.1365-2486.2008.01586.x

Wilson, D., Farrell, C. A., Fallon, D., Moser, G., Müller, C., & Renou-Wilson, F. (2016). Multiyear greenhouse gas balances at a rewetted temperate peatland. *Global Change Biology*, 22, 4080– 4095. https://doi.org/10.1111/gcb.13325

Wood, S. (2017). *Generalized additive models: An introduction with R* ( 2nd ed.). Boca Raton, FL: Chapman & Hall/CRC.

Yang, W. H., & Liptzin, D. (2015). High potential for iron reduction in upland soils. *Ecology*, 96, 2015– 2020. https://doi.org/10.1890/14-2097.1

Ye, R., Espe, M. B., Linquist, B., Parikh, S. J., Doane, T. A., & Horwath, W. R. (2016). A soil carbon proxy to predict $CH_4$ and $N_2O$ emissions from rewetted agricultural peatlands. *Agriculture, Ecosystems & Environment*, 220, 64– 75. https://doi.org/10.1016/j.agee.2016.01.008

Ye, R., Jin, Q., Bohannan, B., Keller, J. K., McAllister, S. A., & Bridgham, S. D. (2012). pH controls over anaerobic carbon mineralization, the efficiency of methane production, and methanogenic pathways in peatlands across an ombrotrophic–minerotrophic gradient. *Soil Biology and Biochemistry*, 54, 36–47. https://doi.org/10.1016/j.soilbio.2012.05.015

Yvon-Durocher, G., Allen, A. P., Bastviken, D., Conrad, R., Gudasz, C., St-Pierre, A., … Del Giorgio, P. A. (2014). Methane fluxes show consistent temperature dependence across microbial to ecosystem scales. *Nature*, 507, 488– 491. https://doi.org/10.1038/nature13164

Zedler, J. B., & Kercher, S. (2005). Wetland resources: Status, trends, ecosystem services, and restorability. *Annual Review of Environment and Resources*, 30, 39– 74. https://doi.org/10.1146/annurev.energy.30.050504.144248

Zeileis, A., & Grothendieck, G. (2005). zoo: S3 infrastructure for regular and irregular time series. *Journal of Statistical Software*, 14, 1– 27.

Zhou, S., Xu, J., Yang, G., & Zhuang, L. (2014). Methanogenesis affected by the co-occurrence of iron(III) oxides and humic substances. *FEMS Microbiology Ecology*, 88, 107– 120. https://doi.org/10.1111/1574-6941.12274